Contrasting photoelectrochemical behaviour of two isomeric supramolecular dyes based on *meso*-tetra(pyridyl)porphyrin incorporating four (μ_3-oxo)- triruthenium(III) clusters

André Luiz Barboza Formiga,[a] Ana Flavia Nogueira,[b] Koiti Araki[c] and Henrique Eisi Toma*[c]

Received (in Durham, UK) 29th June 2007, Accepted 31st January 2008
First published as an Advance Article on the web 17th March 2008
DOI: 10.1039/b709888j

A saddle shaped tetracluster porphyrin species containing four $[Ru_3O(OAc)_6(py)_2]^+$ clusters coordinated to the N-pyridyl atoms of 5,10,15,20-tetra(3-pyridyl)porphyrin, H_2(3-TCPyP), has been investigated in comparison with the planar tetra(4-pyridyl)porphyrin analogue H_2(4-TCPyP). The steric effects from the bulky peripheral complexes play a critical role in the H_2(3-TCPyP) species, determining a non-planar configuration around the porphyrin centre and precluding any significant π-electronic coupling, in contrast with the less hindered H_2(4-TCPyP) species. Both systems exhibit a photoelectrochemical response in the presence of nanocrystalline TiO_2 films, involving the porphyrin excitation around 450 nm. However, only in the H_2(4-TCPyP) case do the cluster moieties also contribute to the photoinduced electron injection process at 670 nm, reflecting the relevance of the electronic coupling between the porphyrin centre and the peripheral complexes.

Introduction

Porphyrins are particularly important prosthetic groups in metalloproteins and enzymes, and their combination with transition metal ions gives rise to a wide range of supramolecular, catalytic, photochemical and self-assembling properties.[1–18] In particular, trinuclear ruthenium clusters provide unique porphyrin modifiers exhibiting a very rich mixed-valence chemistry.[19–21] Their chemistry reflects a peculiar triangular structure held by strong metal–metal bonds, in addition to a central μ_3-oxo-ruthenium and six μ_2-carboxylate-ruthenium bonds. The close proximity of the ruthenium ions provides strong electronic and magnetic interactions, stabilizing a great number of redox states. Previous investigations demonstrated that the supramolecular species obtained by the coordination of (μ_3-oxo)triruthenium(III) clusters to *meso*-tetra(4-pyridyl)metalloporphyrins, M(4-TCPyP), constitute rather versatile catalysts and electrocatalysts.[22–24] For instance, the binding of the ruthenium cluster is responsible for an enhanced cytochrome P450 activity of Mn(4-TCPyP).[23] Rather striking results have been obtained with the Co(4-TCPyP) complex.[24] This species forms stable molecular films on glassy carbon electrodes and exhibits high electrocatalytic efficiency for the 4-electron reduction of dioxygen to water.[24,25]

Therefore, understanding the nature of the electronic effects and structural properties of cluster–porphyrin systems is an important issue to be pursued. In this type of system the bridging group can play a special role, modulating, for instance, the propagation of the electronic effects from the ruthenium cluster residues to the metalloporphyrin site. Besides controlling the electronic interactions, it can also influence the stereochemistry around the porphyrin centre.

Such effects have never been investigated before in ruthenium cluster–porphyrin systems. For this reason, herein, we report on a comparative study of two contrasting isomeric supramolecular species containing four ruthenium cluster units attached to the pyridine N-3 and N-4 atoms of the free base 5,10,15,20-tetra(pyridyl)porphyrin, here denoted H_2(3-TCPyP) and H_2(4-TCPyP), respectively (Fig. 1).

Experimental section

Pyrrole was distilled under vacuum immediately before use. Tetraethylammonium perchlorate ($TEAClO_4$) was prepared by reacting the corresponding hydroxide with perchloric acid, and purified by recrystallization from ethanol.[26] Acetonitrile was distilled and stored in the presence of molecular sieves. All other reagents were analytical grade and used without purification.

5,10,15,20-Tetra(3-pyridyl)porphine, H_2(3-TPyP), was synthesized *via* Rothemund condensation, using a modified Adler procedure.[27,28] 0.75 mL of pyrrole was refluxed with 1.05 mL of 3-pyridinecarboxaldehyde for 90 minutes in 50 mL of glacial acetic acid. The solvent was removed in a flash evaporator and the resulting solid was suspended in a 10% *N,N′*-dimethylformamide–ethanol solution. After few hours, the purple solid was filtered off and washed with ethanol, then with acetone and dried under vacuum, in the presence of silica gel. Elemental analysis for $C_{40}H_{26}N_8{\cdot}C_2H_6O$ Exp. (Calc.): *C* = 76.3 (75.9), H = 4.7 (4.8), N = 17.9 (16.8)%.

[a] *Instituto de Química, Universidade do Estado do Rio de Janeiro, Rio de Janeiro, RJ, Brazil*
[b] *Instituto de Química, Universidade Estadual de Campinas, Campinas, SP, Brazil*
[c] *Instituto de Química, Universidade de São Paulo, P.O. Box 26077, São Paulo, SP, CEP 05513-970, Brazil. E-mail: henetoma@iq.usp.br; Tel: +55 (11) 3091 3887*

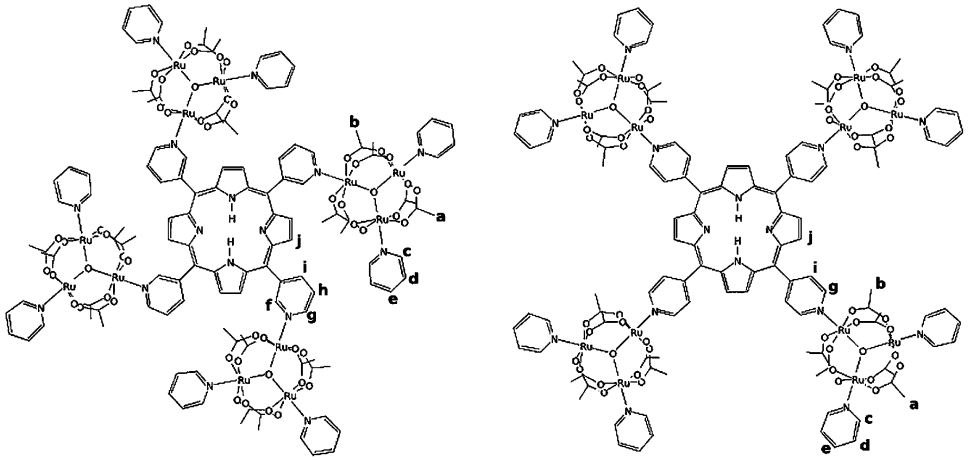

Fig. 1 Structural representations of H_2(3-TCPyP) (left) and H_2(4-TCPyP) (right).

5,10,15,20-Tetra(4-pyridyl)porphine, H_2(4-TPyP), was purchased from Aldrich.

$[Ru_3O(OAc)_6(py)_2(CH_3OH)]PF_6$ (py = pyridine) was synthesized as previously reported.[19,20]

$\{[Ru_3O(OAc)_6(py)_2]_4$(3-TPyP)$\}(PF_6)_4$ or H_2(3-TCPyP): 30 mg of H_2(3-TPyP) was dissolved in 20 mL of 2,2,2-trifluoroethanol and then 200 mg of $[Ru_3O(OAc)_6(py)_2(CH_3OH)]PF_6$, dissolved in 10 mL of the same solvent, was added and stirred for 24 h at room temperature. Then, 50 mL of diethyl ether was added to the mixture and a dark-green solid was collected by filtration. The product was recrystallized in acetonitrile by diffusing diethyl ether into the solution. Finally, it was washed with deionized water, acetone and then diethyl ether, and dried under vacuum in the presence of silica gel. Yield: 42%. Elemental analysis for $C_{128}H_{138}N_{16}O_{52}P_4F_{24}Ru_{12}\cdot 5H_2O$ Exp. (Calc.): C = 33.3 (33.3), H = 3.5 (3.2), N = 4.5 (4.8)%. ES-MS: m/z = 986.5 (3944/4).

H_2(4-TCPyP) or $\{[Ru_3O(OAc)_6(py)_2]_4$(4-TPyP)$\}(PF_6)_4$ was obtained by a similar procedure. Yield 27%. Elemental analysis for $C_{128}H_{138}N_{16}O_{52}P_4F_{24}Ru_{12}\cdot 5H_2O$ Exp. (Calc.): C = 33.5 (33.3), H = 3.3 (3.2), N = 4.9 (4.8)%; ES-MS: m/z = 986.5 (3944/4).

Nanoporous TiO_2 films were prepared from a colloidal solution of TiO_2 (Degussa, P25) according to a previously published procedure.[29] The paste was deposited onto a sheet of F-doped SnO_2 TEC15 conducting glass (sheet resistance $\sim$15 Ω/cm^2) and heated at 450 °C for 30 min. The surface treatment was carried out by immersing the TiO_2 films in 1×10^{-4} mol dm^{-3} solution of the supramolecular species in ethanol, during 48 h. Afterwards, the electrode was washed with the solvent and dried in moisture-free air.

Measurements

The UV-Vis and near-infrared spectra were recorded on a Hewlett-Packard 8453A diode-array spectrophotometer. CV experiments were carried out in 0.1 mol dm^{-3} $TEAClO_4$ acetonitrile solution as supporting electrolyte. An Autolab PGSTAT30 potentiostat/galvanostat and a conventional three electrode cell arrangement consisting of a platinum disk working, a Pt wire auxiliary and $Ag/AgNO_3$ (0.010 mol dm^3, in acetonitrile) reference electrodes were used in all experiments. The potentials were converted to SHE by adding 0.503 V. The spectroelectrochemistry[30,31] experiments were carried out in a homemade thin-layer cell constituted by a gold mini-grid working electrode, a platinum wire auxiliary electrode and $Ag/AgNO_3$ (0.010 mol dm^{-3}, in acetonitrile) reference electrode. The potentials were applied using an EG&G model 173 potentiostat/galvanostat.

NMR spectra were recorded on a Varian 300 MHz INOVA1 spectrometer, in CD_3CN or $CDCl_3$ solutions at room temperature. The reported chemical shifts (δ/ppm) are relative to the signal of the residual protons of the solvent.

The photoelectrochemical cell (1.0 cm^2 active area) was assembled by transferring about 1 mL of the electrolyte solution (0.5 mol dm^{-3} *tert*-butylpyridine, 0.6 mol dm^{-3} tetrabutylammonium iodide, 0.1 mol dm^{-3} LiI, 0.1 mol dm^{-3} I_2 in 10 mL methoxypropionitrile) onto a SnO_2:F^- glass covered with TiO_2/attached dye. The counter electrode was then pressed against the TiO_2/dye film. The transparent counter electrode was prepared separately, by transferring a drop of 0.05 mol dm^{-3} solution of H_2PtCl_6 in isopropanol onto the conducting glass and heating at 400 °C in air for 20 min. A PVC film was placed in between the two electrodes to prevent short circuiting and electrolyte leakage. The assembly was kept together by a clamp. No further sealing was found necessary for the tests described in this work. The photoelectrochemical devices were firmly placed in an optical bench for characterization procedures. The IPCE spectra were obtained using an Oriel Spectral Luminator. The light intensity was varied from 1 to 2 mW cm^{-2}. Photocurrent measurements were performed using a Keithley 610C electrometer. The sample was always illuminated through the conducting glass substrate. The monochromatic light intensity at the electrode position were measured with a Newport Optical Power Meter model 1830-C.

Molecular modeling for H_2(3-TCPyP) and H_2(4-TCPyP) was performed by using a modified MM2 force field, available in the HYPERCHEM package program. A gradient of 10^{-3} kcal mol^{-1} $Å^{-1}$ were used as convergence criterion in a conjugated gradient method.

Results and discussion

Conformational analyses were carried out for the H_2(3-TCPyP) and H_2(4-TCPyP) isomer by varying the rotation angle around the bridging pyridine ring. In the case of H_2(3-TCPyP), three conformations are possible, according to the up and down distribution of the bulky ruthenium cluster moieties, in relation to the porphyrin centre, as illustrated in Fig. 2. The most stable geometry exhibited the peripheral groups in alternating positions, as represented in A, yielding a compact saddle shape configuration. The estimated molecular diameter was 3.0 nm. Configurations B and C exhibited local minimum energies about 2 and 5 kcal mol^{-1} above A, reflecting the contribution of the steric hindrance from the peripheral groups.

In contrast, H_2(4-TCPyP) exhibits only one configuration corresponding to a symmetric, planar distribution of the free rotating cluster moieties around the porphyrin centre (Fig. 3). The corresponding molecular diameter is 3.4 nm, showing an expansion with respect the H_2(3-TCPyP) isomer.

Such contrasting geometries are also reflected in the distinct properties of the two isomers. It should be noticed that while *meso*-tetra(4-pyridyl)porphyrin is insoluble in most conventional solvents, the *meso*-tetra(3-pyridyl)porphyrin isomer is relatively soluble because of its net dipole moment. This is an important aspect that facilitates the synthesis of the tetracluster porphyrins. On the other hand, the tetracluster porphyrin species are much more soluble than the parent pyridylporphyrins, due to the influence of the peripheral groups. Their surprising stability in solvents such as acetonitrile is another important point to be mentioned. In fact, no change in the UV-Vis and ^{1}H-NMR spectral profiles has been observed for the solutions of the tetracluster porphyrins, after two months at room temperature.

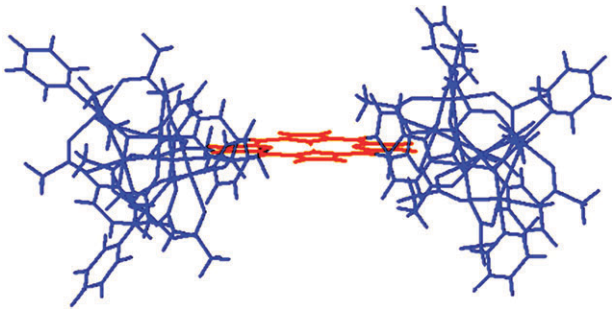

Fig. 3 Optimized geometry (lateral view) for the H_2(4-TCPyP) species.

Electronic spectra

The electronic spectra of the TCPyP species in acetonitrile consist of an envelope of superimposed absorption bands in the 230–850 nm range, arising from the two characteristic porphyrin and cluster chromophore groups. Spectral deconvolution is required to extract the L, N, Soret and Q bands of free-base porphyrins, and the characteristic transitions of the cluster units, *e.g.* the ($\pi \rightarrow \pi^*$)py bands, the four intracluster (IC) bands, and two types of $Ru_3O \rightarrow (\pi^*)$py charge transfer (CLCT) bands, as shown in Fig. 4. By analogy with our previous work[19–24] CLCT(2) was attributed to the charge transfer from Ru_3O unit to the bridging pyridyl–porphyrin groups. The detailed spectroscopic data were collected in Table 1, including the protonated porphyrin and the free TPyP species, for comparison purposes. Such protonated species have been generated by bubbling HCl vapor into the corresponding acetonitrile solutions.

As shown in Table 1, coordination of the ruthenium trinuclear clusters promotes a red shift of the porphyrin absorption bands, either in the neutral free-base or in the protonated forms. A similar behaviour has been reported by Meot-Ner

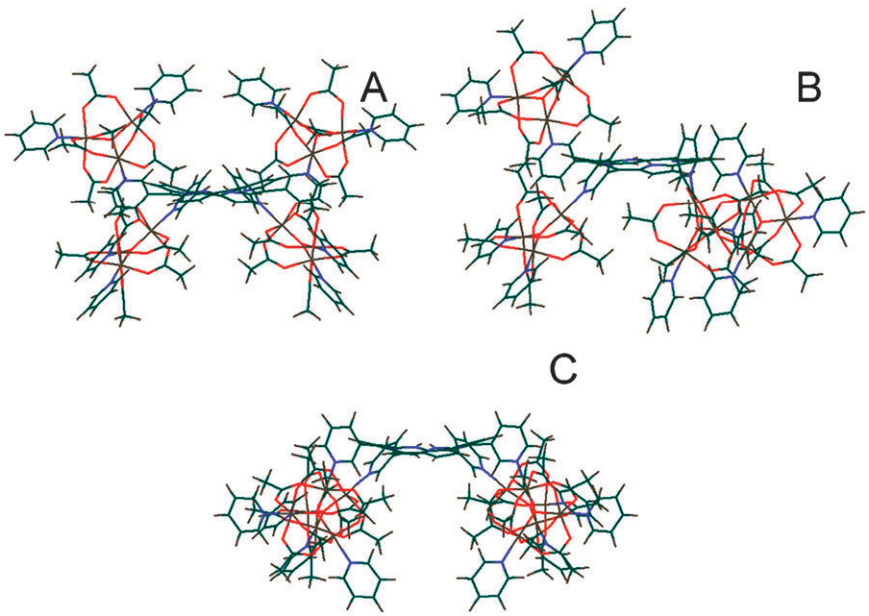

Fig. 2 Three possible configurations for the H_2(3-TCPyP) system (lateral view), showing the most stable geometry (A), and two minimum energy local points represented by B and C.

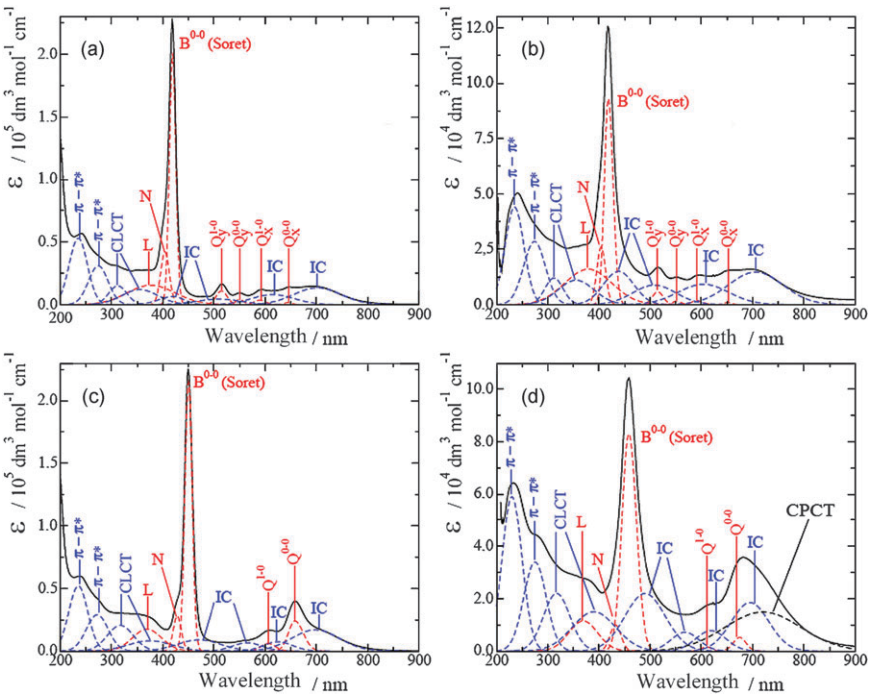

Fig. 4 Experimental and deconvoluted spectra of H_2(3-TCPyP) (a), H_2(4-TCPyP) (b) and their protonated species H_4(3-TCPyP) (c) and H_4(4-H_2TCPyP) (d) in acetonitrile solutions; CLCT = cluster-to-ligand charge transfer, IC = intra-cluster and CPCT = cluster-to-porphyrin charge transfer transition.

and Adler[32] for the substitution effect in the phenyl ring of tetraphenylporphyrins and interpreted on the basis of Gouterman's four-orbital model.[33,34] According to this model, the symmetric substitution at the *meso* positions should mainly influence the HOMO a_{2u} orbital, so that the red shift induced by electron withdrawing groups reflects the energy increase of that orbital. Based on the molecular orbital diagram for the Ru_3O core proposed by Baumann and Meyer,[35] the cluster HOMO can be represented by a half filled a_2' π orbital, considering a D_{3h} local symmetry. This orbital overlaps the π* orbital of the pyridyl bridging group and of the porphyrin ring. However, the extent of orbital overlap should depend on the dihedral angle between the molecular planes involved.

In the case of H_2(4-TCPyP), according to the molecular simulations, the occurrence of π-electronic coupling is rather plausible, since the cluster moieties exert little influence on the free rotation of the bridging pyridine group. In contrast, in the case of the sterically hindered H_2(3-TCPyP) species, both the position of the pyridine N-atom, and orthogonal orientation of the cluster groups with respect to the porphyrin ring, can prevent the occurrence of effective π-electronic coupling. This fact seems to be reflected in the narrower spectral bandwidth for the H_2(3-TCPyP) isomer, as shown in Fig. 4. In this case, the coordination of the ruthenium trinuclear clusters to the pyridine N-atoms causes only a small broadening of the Soret band ($\Delta\nu_{1/2}$ = 975.7 cm^{-1}, as compared with $\Delta\nu_{1/2}$ = 760.5 cm^{-1} for the starting free-base). In the case of H_2(4-TCPyP),

Table 1 Electronic spectroscopy data (λ/nm; log ε) for *meso*-tetrapyridylporphyrins and their modified cluster species, in the free-base and diprotonated forms

	Soret	$Q_{y(1,0)}$	$Q_{y(0,0)}$	$Q_{x(1,0)}$	$Q_{x(0,0)}$	π → π*		CLCT(1)	CLCT(2)	IC(4)	IC(3)	IC(2)	IC(1)	CPCT
Ru_3OL_3[a]						232(4.3)	272(4.0)	320(3.7)		375(3.5)	511(3.2)	615(3.5)	704(3.7)	
H_2(3-TPyP)[b]	414(5.6)	512(4.2)	544(3.8)	587(3.7)	643(3.4)									
H_4(3-TPyP)[b]	433(5.4)			582(3.9)	632(4.2)									
H_2(4-TPyP)[c]	417(5.6)	513(4.3)	547(3.7)	588(3.8)	643(3.2)									
H_4(4-TPyP)[b]	442(5.5)			588(4.1)	640(4.2)									
H_2(3-TCPyP)[d]	419(5.3)	515(4.0)	550(3.6)	589(3.6)	645(3.2)	235(4.7)	274(4.5)	312(4.2)	355(4.1)	420(3.8)	510(3.7)	615(3.9)	702(4.1)	
H_4(3-TCPyP)[d]	450(5.3)			606(3.8)	658(4.4)	235(4.7)	272(4.5)	317(5.3)	375(3.9)	471(4.0)	565(3.8)	625(3.9)	698(4.2)	
H_2(4-TCPyP)[d]	418(5.0)	515(3.8)	552(3.2)	591(3.2)	652(3.0)	235(4.6)	274(4.5)	312(4.1)	355(4.0)	438(4.2)	508(3.9)	604(4.0)	706(4.2)	
H_4(4-TCPyP)[d]	458(4.9)			610(3.2)	675(3.7)	230(4.8)	275(4.5)	317(4.3)	390(4.2)	490(4.3)	568(3.9)	619(3.9)	695(4.3)	720(4.2)

[a] $[Ru_3O(OAc)_6(py)_3]^+$. [b] Protonated species in aqueous solution. [c] In $CHCl_3$. [d] In CH_3CN. Values were obtained from spectral deconvolution. CLCT = cluster-to-ligand charge transfer; IC = intra-cluster transition; CPCT = cluster-to-porphyrin charge transfer transition.

an extensive broadening (more than 100%) is observed, reflecting the influence of the electronic coupling between the porphyrin and the peripheral cluster groups.

Considering the spectra of the protonated species shown in Fig. 4(c) and 4(d), it should be noted that the spectral pattern for H_4(3-TCPyP) is essentially composed by the superimposition of the absorption bands the Ru_3O cluster and the protonated H_4(3-TPyP) chromophores. The Soret band is shifted to lower energy (Table 1) with little broadening ($\Delta\nu_{1/2}$ = 889.2 cm^{-1}) and the four band pattern in the visible changes into a two band pattern, characteristic of the protonated porphyrin ring, while the cluster bands remain unchanged (Fig. 4c and Table 1). In contrast, protonation of the H_2(4-TCPyP) isomer promotes more extensive Soret band broadening ($\Delta\nu_{1/2}$ = 1997.8 cm^{-1}) and appearance of a new, broad and quite intense band at 720 nm, superimposed to the intracluster and Q bands (Fig. 4d). In general, it is known that protonation leads to a distortion of the porphyrin ring to a saddle shape configuration, decreasing the steric hindrance between the *ortho*-hydrogen atoms of the pyridyl bridge and the β-pyrrole hydrogen atoms. This favors the π-electronic coupling between the cluster and the protonated porphyrin ring, and explains the occurrence of a new charge-transfer band, here denoted CPCT, at 720 nm in Fig. 4d. This band has been unequivocally detected in the spectrum of the protonated $H_4\{4\text{-TPyP}(Ru^{II}(bipy)_2Cl)_4\}^{6+}$ complex,[31] since in this case, there is no interference from the broad absorption bands of the ruthenium cluster moieties. No such band has been observed in the corresponding $H_4\{3\text{-TPyP}(Ru^{II}(bipy)_2Cl)_4\}^{6+}$ isomer.[15] On the other hand, spectroelectrochemical measurements (not shown) carried out for the 4-TCPyP system have confirmed that the 670 nm band is associated with a cluster–porphyrin transition, rather than to a porphyrin Q band, since it completely disappears when the cluster moieties are oxidized.

NMR spectroscopy

The ^1H NMR spectra of the H_2(3-TCPyP), H_2(4-TCPyP), $[Ru_3O(CH_3CO_2)_6(py)_3]^+$, H_2(3-TPyP) and H_2(4-TPyP) species were assigned based on their corresponding ^1H–^1H COSY data, and were compiled in Table 2 for comparison purposes.

In comparison with the model $[Ru_3O(CH_3CO_2)_6(py)_3]^+$ cluster,[36,37] the signals associated with the bridging acetate ligands were split, reflecting two different chemical environments, as expected for clusters with C_{2V} local symmetry. Furthermore, a decrease in the bridging pyridyl proton signal was observed, due to the paramagnetic effects of the peripheral ruthenium clusters and the conformational changes caused by the rotation of the pyridyl bridge. All cluster signals of the H_2(3-TCPyP) species were shifted up-field in comparison with the corresponding signals in the H_2(4-TCPyP) isomer (Table 2). This behaviour is associated with the position of the cluster units relative to the porphyrin ring in those supermolecules. In fact, in the H_2(3-TCPyP) they are located either above or below the porphyrin plane, but always in a closer distance to it in comparison with the H_2(4-TCPyP) isomer. Consequently, the cluster units are subjected to more intense magnetic shielding by the porphyrin ring current effects.[38–42] The H_f proton was not detected, because of the strong broadening induced by the local paramagnetic effects.

The β-pyrrolic protons H_j appear as an intense singlet at 6.41 ppm (8H) in the ^1H-NMR spectrum of H_2(3-TCPyP). This signal can be used to probe the symmetry of the porphyrin ring. The presence of only one well defined peak is a strong evidence that all those protons experience an equivalent chemical environment and that the molecule is symmetric. The N–H pyrrolic protons appear as a broadened singlet at −3.74 ppm (2H) and are very sensitive to core substitution. Consequently, those singlet peaks confirm the presence of just one symmetric species in solution. This evidence, in conjunction with the relative simplicity of the spectrum and the observed paramagnetic shifts, support the coordination of four ruthenium clusters to each porphyrin ring. The magnetic equivalence of all β-pyrrolic signals due to pyridyl rotation and the equivalence of N–H protons due to rapid intramolecular proton exchange (hydrogen bonding), explain the spectral pattern of an overall D_{4h} symmetry for the porphyrin core at least in the NMR time scale, at room temperature.[38]

By comparing the data for the species in Table 2, the shielding of the N–H proton signal follows the sequence H_2(4-TCPyP) > H_2(3-TCPyP) > H_2(4-TPyP) > H_2(3-TPyP). This is associated with the porphyrin ring current: the more negative is its value, the greater is the ring current.[38] Analyzing the observed trends, one can conclude that the coordination of the ruthenium clusters induces an increase in the ring current which depends on the N-substitution position. Presumably, in H_2(3-TPyP) it is not so effective as in the H_2(4-TPyP) isomer, as a consequence of the stronger π-interaction in the last one.

Table 2 ^1H chemical shifts for the H_2(3-TCPyP), H_2(4-TCPyP), H_2(3-TPyP), H_2(4-TPyP) and $[Ru_3O(CH_3CO_2)_6(py)_3]^+$ cluster species, in CD_3CN or $CDCl_3$

Signal[c]	3-TCPyP	4-TCPyP	3-TPyP[a]	4-TpyP[25a]	Ru_3OL_3[19]
a	4.84	5.10			
b	4.90	4.98			4.82
c	−1.41	0.20			0.25
d	4.82	5.82			5.82
e	6.07	6.61			6.57
f	n.o.[b]		9.46		
g	0.22	0.91	9.07	9.04	
h	5.82		7.77		
i	6.57	6.39	8.53	8.18	
j	6.41	7.77	8.87	8.82	
NH	−3.74	−4.00	−2.82	−2.95	

[a] In $CDCl_3$ solution. [b] Not observed. [c] Labels shown in Fig. 1.

Electrochemistry and spectroelectrochemistry

Cyclic voltammetry of H_2(3-TCPyP) exhibits the typical electrochemical pattern of the cluster moieties and is very similar to that of the isomer H_2(4-TCPyP)[22] (Fig. 5). Four intense waves in the −1.5 to 2.4 V range (Table 3) were ascribed to successive redox couples formally represented as $Ru_3^{III,II,II}O$/$Ru_3^{III,III,II}O$/$Ru_3^{III,III,III}O$/$Ru_3^{IV,III,III}O$/$Ru_3^{IV,IV,III}O$ by comparison with previously reported systems.[37] The first three processes are typically reversible and the peak currents exhibit a linear dependence on the concentration and on the square root of the scan rates.[26] Also, two processes involving the porphyrin ring were observed: a reversible wave at −0.73 V

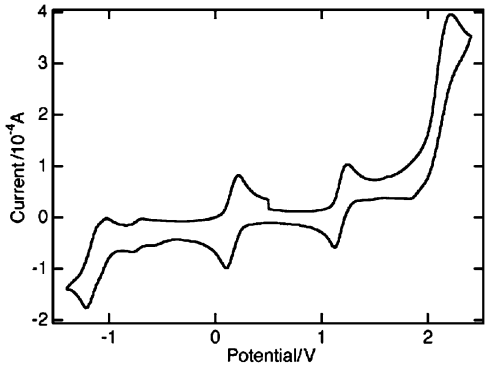

Fig. 5 Cyclic voltammogram of 3-TCPyP in acetonitrile (2.0×10^{-3} mol dm^{-3}), $TEAClO_4$ 0.1 mol dm^{-3} at 50 mV s^{-1} in the −1.5 to 2.4 V range.

and a shoulder at −1.03 V corresponding to the first and second reduction of the porphyrin ring. The last one is hardly seen in the voltammogram, but has been confirmed spectroelectrochemically.

The oxidation of the H_2(3-TCPyP) solution in the 1.12 to 1.32 V potential range shifted the intracluster transition band from 700 to 800 nm and led to a small decrease of the Soret band at 419 nm (Fig. 6a). A further increase of the potential (1.40 V range) promoted a major change in the porphyrin spectrum (Fig. 6b). The Soret band was shifted from 419 to 438 nm concomitantly with the rise of a new band at 648 nm, while the intracluster transition at 800 nm remained unchanged. This behaviour is consistent with the occurrence of two successive oxidation processes, one localized on the ruthenium cluster and the other one on the porphyrin ring, respectively, generating the radical cation. At 1.6 V, the beginning of the porphyrin second oxidation reaction can be observed from the decay of the radical cation species around 430 nm (not shown), before the oxidation of the ruthenium cluster to the $Ru_3^{IV,IV,III}O$ state at 2.2 V. The measurements above 2.2 V were precluded by the current overflow at the limit of the solvent window, presumably containing traces of humidity.

The reduction processes below 0.5 V are shown in Fig. 7, and exhibit quite similar spectral changes for both isomers. The reversible reduction of the peripheral clusters is responsible for the shift of the intracluster bands from 700 to 900 nm, in the low energy part of the spectrum, in parallel with a small decrease in the intensity of the Soret band, Fig. 7(a). This decrease is significant since it is observed in spite of the rise of a MLCT band associated with the cluster units at the same spectral region. The first reduction of the porphyrin ring was observed in the −0.30 to −0.46 V range, associated with a shift of the Soret band from 419 to 447 nm, the fading of the Q band at 514 nm and the appearance of a new broad absorption around 600 nm, Fig. 7(b). No significant changes were observed in the cluster absorption bands during that process. The second reduction of the porphyrin ring, yielding dianionic species, takes place at potentials in the −0.85 to −1.14 V range. The intensity of the Soret band at 447 nm steadily decreased before the beginning of the changes in the characteristic intracluster band envelope in the 600–900 nm range, Fig. 7(c), generating the $Ru_3^{III,II,II}O$ species.

Table 3 Electrochemical data (in V) of H_2(3-TCPyP), H_2(4-TCPyP) and $[Ru_3O(OAc)_6(py)_3]^+$ species in acetonitrile solution

Process	3-TCPyP	4-TCPyP[22]	Ru_3O[43]
$Ru_3O^{III,III,II/III,II,II}$	−1.15	−1.14	−1.08
$P^{1-/2-}$	−1.03	−1.05	
$P^{0/1-}$	−0.73	−0.72	
$Ru_3O^{III,III,III/III,III,II}$	0.17	0.16	0.19
$Ru_3O^{IV,III,III/III,III,III}$	1.19	1.23	1.21
$P^{1/0}$	1.55	1.68	
$Ru_3O^{IV,IV,III/IV,III,III}$	2.21	2.30	2.17

The redox potentials of H_2(3-TCPyP), H_2(4-TCPyP) and $[Ru_3O(OAc)_6(py)_3]^+$ species are summarized in Table 3.

Photoelectrochemistry

Since the remarkable work of O'Reagan and Grätzel[44] in 1991, dye sensitized solar cells (DSC) have been increasingly investigated as a promising alternative for cheap solar energy conversion.[45–50] Such devices are based on molecular dyes attached to nanoporous nanoparticulate TiO_2. They efficiently make use of the dye capability to inject photoexcited electrons into the conduction band of TiO_2. Completion of the electrical circuit is achieved by an electrolyte containing a redox mediator/hole conducting material into the film pores.

A critical review of the state-of-art research in this field has been recently published by a European consortium.[51] Among

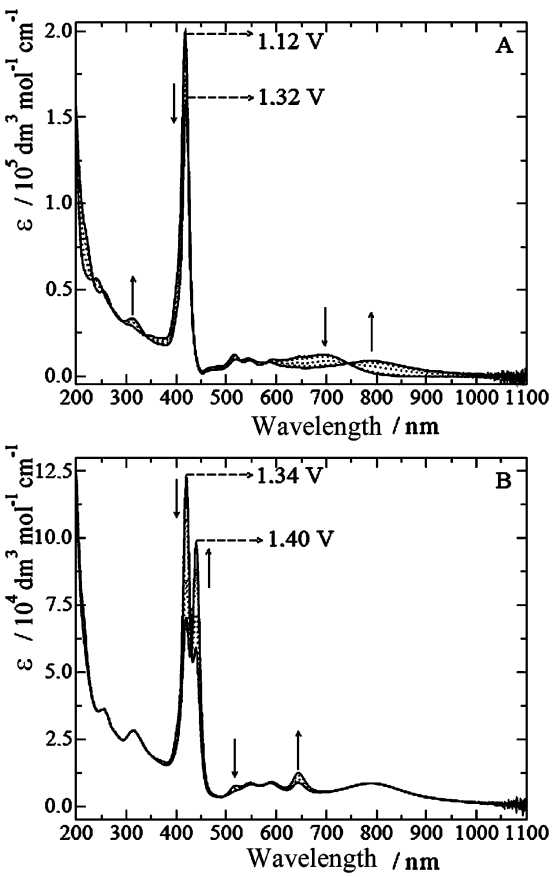

Fig. 6 Spectroelectrochemistry of H_2(3-TCPyP) in the 1.12 to 1.32 (a) and 1.34 to 1.40 V range (b), in 1×10^{-5} mol dm^{-3} acetonitrile solution.

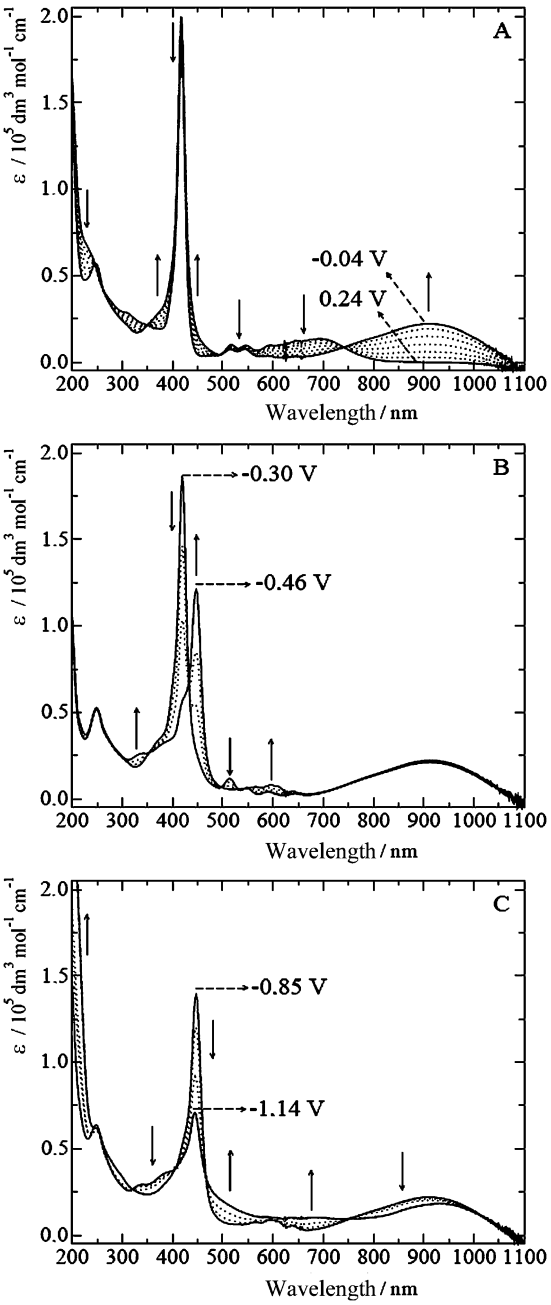

Fig. 7 Spectroelectrochemistry of H_2(3-TCPyP) in the 0.24 to −0.04 V (a); −0.30 to −0.46 V (b) and −0.85 to −1.14 V (c) ranges, in 1×10^{-5} mol dm^{-3} acetonitrile solution.

the many challenges listed in this review paper, one of the factors currently limiting device performance is the inefficient light absorption by existing sensitizer dyes in the near infrared, *e.g.* above 700 nm. In this sense, the use of a mixture of dyes, or supramolecular systems combining suitable complementary chromophore groups, has been proposed.[52,53] Following this approach, several supramolecular porphyrins and polynuclear ruthenium complexes have been investigated in our laboratory, some of them exhibiting remarkable photoelectrochemical response.[54–57]

Because of their absorption profiles which extend up to the NIR region, the tetracluster porphyrins provide interesting prototype supramolecular species to be tested in DSC, regarding their relative behaviour as photoinjectors and their molecular structure characteristics. The use of protonated species were here preferred, because of their strong absorption bands in the near-infrared region. Our focus was mainly concentrated on the relative performance of these isomeric supramolecular dyes, rather than on their absolute efficiencies. This will require the use of suitable TiO_2 anchoring groups[45] (*e.g.* carboxylate) either in H_2(3-TCPyP) or H_2(4-TCPyP), and is part of our future investigation.

Exploratory experiments with the H_4(3-TCPyP) and H_4(4-TCPyP) based DSC devices revealed indeed an interesting photoelectrochemical behaviour, as shown in Fig. 8. The corresponding IPCE spectra are rather informative, since they describe the monochromatic photon-to-electron conversion efficiency as a function of wavelength, showing the contribution of the several components of the supramolecular species to the measured photocurrent.

As one can see in Fig. 8, both H_4(3-TCPyP) and H_4(4-TCPyP) based DSC exhibit similar photoelectrochemical response in the 400–550 nm region, involving the excitation at the porphyrin Soret band. However only H_4(4-TCPyP) exhibits a photo-action response in the 600–800 nm region, coinciding with the CPCT band. No similar response has been observed for DSC based on nanocrystalline TiO_2 modified with ruthenium acetate clusters[57] or porphyrin species.[56]

On the other hand, in the case of H_4(3-TCPyP), only the porphyrin unit is able to inject photo-electrons into the TiO_2 conduction band. The observed IPCE values in the 400–600 nm region are slightly higher than for the H_4[4-TCPyP] analogue (Fig. 8). This observation may be related to the stronger absorptivity of the porphyrin Soret band in H_4(3-TCPyP) isomer, (Table 1) and the more compact packing of the molecules due to their smaller diameter, thus increasing the surface concentration. The observed IPCE profile is also in agreement with a rather weak electronic coupling between the two components of the supermolecule. In the case of the H_4(4-TCPyP) species, both porphyrin and cluster units participate in the photoinduced electron transfer process, corroborating the importance of the electronic interactions in supramolecular dyes for DSC applications.

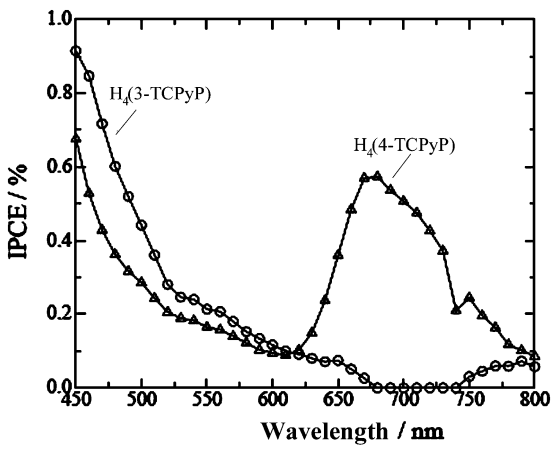

Fig. 8 IPCE *vs.* λ curves for the DSC assembled with the protonated supramolecular species H_4(4-TCPyP) (■) and H_4(3-TCPyP) (○).

Final remarks

According to the molecular modeling simulations, electronic and ^{1}H-NMR spectra and the electrochemical data for the H_2(3-TCPyP) and H_4(4-TCPyP) species, the electronic coupling and electron density on the porphyrin core can be influenced by the coordination of $[Ru_3O(OAc)_6(py)_2]^+$ complexes to the pyridyl N-atoms of H_2(TPyP). This is particularly evident in the protonated H_4(4-TCPyP) supermolecule, in which case a new band at 720 nm ascribed to a cluster-to-porphyrin charge-transfer transition has been detected, corroborating a previous observation for the related $H_4\{4\text{-TPyP}(Ru^{II}(bipy)_2Cl)_4\}^{6+}$ complex.[31] Sensitization of nanoporous TiO_2 films by the tetracluster porphyrin species has been demonstrated, involving photo-injection from direct excitation at the porphyrin Soret band. A new excitation profile in the near-infrared region, coinciding with the cluster-to-porphyrin charge-transfer transition at 670 nm, has been observed in the H_2(4-TCPyP) case, reflecting the important role of the electronic coupling in this system.

Acknowledgements

The support from Fundação de Amparo à Pesquisa do Estado de São Paulo (FAPESP), Conselho Nacional de Desenvolvimento Científico e Tecnológico (CNPq) and Instituto do Milênio de Materiais Complexos (IM2C), is gratefully acknowledged.

References

1. K. Araki and H. E. Toma, Supramolecular porphyrins as electrocatalysts, in *N-4 Macrocyclic Metal Complexes*, ed. J. H. Zagal, F Bedioui and J.-P. Dodelet, Springer, 2006, pp. 255–302.
2. H. E. Toma and K. Araki, *Coord. Chem. Rev.*, 2000, **196**, 307.
3. L. Latos-Grazynski, K. Rachlewicz and J. Wojaczynski, *Coord. Chem. Rev.*, 1999, **192**, 109.
4. T. Imamura and K. Fukushima, *Coord. Chem. Rev.*, 2000, **198**, 133.
5. J. K. M. Sanders, in *The Porphyrin Handbook*, ed. K. M. Kadish, *et al.*, Academic Press, New York, 2000.
6. J. C. Chambron, V. Heitz and J. P. Sauvage, in *The Porphyrin Handbook*, ed. K. M. Kadish, *et al.*, Academic Press, New York, 2000.
7. L. Baldini and C. A. Hunter, *Advances in Inorganic Chemistry*, Vol. 53, 2002.
8. A. Prodi, M. T. Indelli, C. J. Kleverlaan, E. Alessio and F. Scandola, *Coord. Chem. Rev.*, 2002, **229**, 51.
9. N. Rea, B. Loock and D. Lexa, *Inorg. Chim. Acta*, 2001, **312**, 53.
10. I. Mayer, G. Nunes and H. E. Toma, *Eur. J. Inorg. Chem.*, 2006, **4**, 850.
11. M. S. Quintino, K. Araki and H. E. Toma, *Talanta*, 2006, **4**(68), 1281.
12. H. Winnischofer, H. E. Toma and K. Araki, *J. Nanosci. Nanotechnol.*, 2006, **6**, 1701.
13. I. Mayer, M. Nakamura, H. E. Toma and K. Araki, *Electrochim. Acta*, 2006, **52**, 263.
14. H. E. Toma and K. Araki, *J. Chem. Res. (S)*, 1990, 82.
15. I. Mayer, A. L. B. Formiga, F. Engelmann, H. Winnischofer, P. V. Oliveira, D. M. Tomazella, H. E. Toma, M. N. Eberlin and K. Araki, *Inorg. Chim. Acta*, 2005, **358**, 2629.
16. M. S. Quintino, H. Winnischofer, M. Nakamura, H. E. Toma, K. Araki and L. Angnes, *Anal. Chim. Acta*, 2005, **539**, 215.
17. G. Nunes, I. Mayer, H. E. Toma and K. Araki, *J. Catal.*, 2005, **236**, 55.
18. K. Araki, H. Winnischofer, H. E. Viana, M. M. Toyama, F. Engelmann, I. Mayer, A. L. B. Formiga and H. E. Toma, *J. Electroanal. Chem.*, 2004, **562**, 145.
19. H. E. Toma, K. Araki, A. D. P. Alexiou, S. Nikolaou and S. Dovidauskas, *Coord. Chem. Rev.*, 2001, **219**, 187.
20. H. E. Toma and C. Cipriano, *J. Electroanal. Chem.*, 1989, **263**, 313.
21. H. E. Toma, F. M. Matsumoto and C. Cipriano, *J. Electroanal. Chem.*, 1993, **346**, 261.
22. H. E. Toma, K. Araki and E. O. Silva, *Monatsh. Chem.*, 1998, **129**, 975.
23. S. Dovidauskas, H. E. Toma, K. Araki, H. C. Sacco and Y. Iamamoto, *Inorg. Chim. Acta*, 2000, **305**, 206.
24. K. Araki, S. Dovidauskas, H. Winnischofer, A. D. P. Alexiou and H. E. Toma, *J. Electroanal. Chem.*, 2001, **498**, 152.
25. H. Winnischofer, V. Y. Otake, S. Dovidauskas, M. Nakamura, K. Araki and H. E. Toma, *Electrochim. Acta*, 2004, **49**, 3711.
26. D. T. Sawyer and J. L. Roberts, *Experimental Electrochemistry for Chemists*, Wiley, 1974.
27. A. D. Adler, F. R. Longo, J. d. Finarell, J. Goldmach, J. Assour and L. Korsakof, *J. Org. Chem.*, 1967, **32**, 476.
28. K. Kalyanasundaram, *Inorg. Chem.*, 1984, **23**, 2453.
29. M. K. Nazeeruddin, A. Kay, R. Humphry-Baker, E. Muller, P. Liska, N. Vanchopoulos and M. Grätzel, *J. Am. Chem. Soc.*, 1993, **115**, 6382.
30. K. Araki and H. E. Toma, *Cur. Org. Chem.*, 2002, **6**, 21.
31. K. Araki and H. E. Toma, *J. Coord. Chem.*, 1993, **30**, 9.
32. M. Meot-Ner and A. D. Adler, *J. Am. Chem. Soc.*, 1975, **97**, 5107.
33. M. Gouterman, *J. Mol. Spectrosc.*, 1961, **6**, 138.
34. M. Gouterman, L. C. Snyder and G. H. Wagniere, *J. Mol. Spectrosc.*, 1963, **11**, 108.
35. J. A. Baumann, D. J. Salmon, S. T. Wilson, T. J. Meyer and W. E. Hatfield, *Inorg. Chem.*, 1978, **17**, 3342.
36. A. D. P. Alexiou and H. E. Toma, *J. Chem. Res. (S)*, 1997, 338.
37. H. E. Toma and A. D. P. Alexiou, *J. Chem. Res. (S)*, 1995, 134.
38. T. R. Janson and J. J. Katz, in *Nuclear Magnetic Resonance of Diamagnetic Porphyrins*, ed. D Dolphin, Academic Press, 1979.
39. A. V. Chernook, U. Rempel, C. vonBorczyskowski, A. M. Shulga and E. I. Zenkevich, *Chem. Phys. Lett.*, 1996, **254**, 229.
40. E. Alessio, S. Geremia, S. Mestroni, E. Iengo, I. Srnova and M. Slouf, *Inorg. Chem.*, 1999, **38**, 869.
41. E. Alessio, S. Geremia, S. Mestroni, I. Srnova, M. Slouf, T. Gianferrara and A. Prodi, *Inorg. Chem.*, 1999, **38**, 2527.
42. E. B. Fleischer and A. M. Shachter, *Inorg. Chem.*, 1991, **30**, 3763.
43. A. D. P. Alexiou and H. E. Toma, *J. Chem. Res. (S)*, 1993, 464.
44. B. O'Reagan and M. Grätzel, *Nature*, 1991, **353**, 737.
45. M. K. Nazeeruddin, R. Humphry-Baker, P. Liska and M. Gratzel, *J. Phys. Chem. B*, 2003, **107**, 8981.
46. P. Wang, S. M. Zekeeruddin, J. E. Moser, R. Humphry-Baker, P. Comte, V. Aranyos, A. Hagdeldt, M. K. Nazeeruddin and M. Gratzel, *Adv. Mater.*, 2003, **16**, 1806.
47. S. A. Haque, E. Palomares, B. M. Cho, A. N. M. Green, N. Hirata, K. R. Klug and J. R. Durrant, *J. Am. Chem. Soc.*, 2005, **127**, 3456.
48. H. Tributsch, *Coord. Chem. Rev.*, 2004, **248**, 1511.
49. U. Wurfel, J. Wagner and A. Hinsch, *J. Phys. Chem. B*, 2005, **109**, 20444.
50. M. Durr, A. Bamedi, A. Yasuda and G. Nelles, *Appl. Phys. Let.*, 2004, **84**, 3397.
51. J. M. Kroon, N. J. Bakker, H. S. P. Smit, P. Liska, K. R. Thampi, P. Wang, S. M. Zakeeruddin, M. Gratzel, A. Hinsch, S. Hore, U. Wurfel, R. Sastrawan, J. R. Durrant, E. Palomares, H. Pettersson, T. Gruszecki, J. Walter, K. Skupien and G. E. Tulloch, *Prog. Photovolt: Res. Appl.*, 2007, **15**, 1.
52. C. A. Bignozzi, R. Argazzi, M. T. Indelli and F. Scandola, *Sol. Energy Mater. Sol. Cells*, 1994, **32**, 229.
53. D. S. Haque, S. Handa, K. Peter, E. Palomares, M. Thelakkat and J. R. Durrant, *Angew. Chem., Int. Ed.*, 2005, **44**, 5740.
54. A. F. Nogueira, S. H. Toma, M. Vidotti, A. L. B. Formiga, S. I. C. Torresi and H. E. Toma, *New J. Chem.*, 2005, **29**, 320.
55. A. F. Nogueira, L. F. O. Furtado, A. L. B. Formiga and H. E. Toma, *Inorg. Chem.*, 2004, **43**, 396.
56. A. F. Nogueira, A. L. B. Formiga, H. Winnischofer and H. E. Toma, *Photochem. Photobiol. Sci*, 2004, **3**, 56.
57. L. F. O. Furtado, A. D. P. Alexiou, L. Gonçalves, H. E. Toma and K. Araki, *Angew. Chem., Int. Ed.*, 2006, **45**, 3143.

